9096 *Biochemistry* **2010,** *49,* 9096–9105
DOI: 10.1021/bi101069u

BIOCHEMISTRY
including biophysical chemistry & molecular biology
Article

Understanding the Molecular Activity of Alkaline Sphingomyelinase (NPP7) by Computer Modeling[†]

Jianxin Duan,*[,‡] Jun Wu,[§] Yajun Cheng,[∥] and Rui-Dong Duan[∥]

[‡]*Schrödinger GmbH, Dynamostrasse 13, 681 61 Mannheim, Germany,* [§]*Beijing Institute of Biotechnology, Beijing 100071, China, and* [∥]*Biomedical Center B11, Lund University, S-221 85 Lund, Sweden*

Received July 4, 2010; Revised Manuscript Received September 9, 2010

ABSTRACT: The enzymes in the nucleotide pyrophosphatase/phosphodiesterase (NPP) family have various substrates such as nucleotides, phospholipids, and sphingolipids. The substrate specificity in relation to their structures is largely unknown because no mammalian NPP complex has been crystallized. NPP7, also called alkaline sphingomyelinase (alk-SMase), is a NPP family member that may have important implications in carcinogenesis and cholesterol absorption. The sequence of NPP7 is 36% similar to that of the closest NPP member, but NPP7 has no activity against nucleotides. In this work, we predict the three-dimensional structure of NPP7 by homology modeling using a recently crystallized NPP from bacteria. Using the model, we studied the substrate specificity of the enzyme by docking. The model generated explains the functional changes in previous mutagenesis studies and rationalizes the structural basis for the lack of activity toward nucleotides. An effort to shift the substrate specificity from sphingomyelin (SM) to nucleotide was not successful but revealed a site-directed mutation that increased activity toward SM. In conclusion, this is the first study to predict the structure of a mammalian NPP and its substrate specificity by molecular modeling. The information may be helpful in understanding the functional differences of NPP members.

Alkaline sphingomyelinase (alk-SMase)[1] was identified by Nilsson in 1969 (*1*) and purified and cloned by Duan et al. in 2003 (*2*). The enzyme can cleave the phosphocholine headgroup from several phospholipids, including sphingomyelin (SM), platelet activating factor (PAF), and lysophosphatidylcholine (lyso-PC), by a phospholipase C activity (*2*, *3*). The enzyme may prevent carcinogenesis by different mechanisms, such as generating the proapoptotic molecule ceramide, inactivating the proinflammatory molecule PAF, and reducing the level of formation of the proliferative and angiogenic molecule lysophosphatidic acid (LPA), as recently reviewed (*4*). Significant reduction of alk-SMase activity has been found in human colorectal adenoma, colorectal carcinoma, and colitis (*5*−*7*). Abnormal forms of alk-SMase induced by alternative splicing have been identified in human colon and liver cancer cell lines (*8*, *9*). In agreement with the anticancer and antiinflammatory effect of alk-SMase, recombinant alk-SMase was recently shown to suppress the inflammatory response by inhibiting TNF-α expression in the colon in animal studies (*10*), and the expression of the enzyme could be upregulated by dietary SM (*11*) and by certain probiotics that have antiinflammatory effects (*12*).

Bioinformatics studies showed that alk-SMase shares no sequence similarity with other SMases but belongs to the nucleotide pyrophosphatase/phosphodiesterase (NPP) family (*2*). The human NPP family so far has seven members, and alk-SMase is the newest addition and is therefore called NPP7 (*13*). Until a few years ago, NPPs were only known to hydrolyze pyrophosphate or phosphodiester bonds in (di)nucleotides and their derivatives. However, the discoveries of NPP6 (*14*) and NPP7 (alk-SMase) (*2*) showed that some NPPs could hydrolyze phospholipids containing a choline headgroup, such as SM and lyso-PC. Several important functions of NPPs have been identified depending on their substrate specificity and locations. NPP1, by generating pyrophosphate (PP_i), inhibits bone mineralization and induces insulin resistance (*13*). NPP2 is identical to autotaxin, an extracellular lysophospholipase D that hydrolyzes lyso-PC to generate LPA, which stimulates cell proliferation and migration. NPP3 is enriched in basophiles and involved in allergy. NPP6 can hydrolyze lyso-PC by a phospholipase C activity and thus affect the formation of LPA (*14*). The functions of NPP4 and NPP5 are currently unknown as their specific substrates have not yet been identified.

As shown in Table 1, an obvious property of NPP family members is the substrate specificity. Some like NPP1 and NPP3 have activity against only nucleotides and their derivatives, while others like NPP6 and NPP7 have no activity against nucleotides but high activity against phospholipids containing a phosphocholine headgroup (*15*). NPP2 is the member that has activity against both nucleotides and lysophospholipids. Even among those with activity against phospholipids, NPP2 cleaves the choline headgroup from lyso-PC and thus has lysophospholipase D activity, and others like NPP6 and NPP7 cleave phosphocholine and thus have phospholipase C activity. NPP7 is the only

[†]The cell biological studies were supported by grants from Swedish Cancer Society, the Albert Pahlsson Foundation, and the Research Foundation of Lund University Hospital.

*To whom correspondence should be addressed. E-mail: jianxin.duan@schrodinger.com. Telephone: +49 621 43855 172. Fax: +49 621 43855 555.

[1]Abbreviations: alk-SMase, alkaline sphingomyelinase; SM, sphingomyelin; NPP, nucleotide pyrophosphatase/phosphodiesterase; PAF, platelet activating factor; lyso-PC, lysophosphatidylcholine; PC, phosphatidylcholine; LPA, lysophosphatidic acid; APBS, Adaptive Poisson−Boltzmann Solver; OD, optical density; dpm, disintegrations per minute; P_i, phosphate; PP_i, pyrophosphate; AMP, adenosine monophosphate; PCR, polymerase chain reaction; pNTMP, thymidine 5′-monophosphate *p*-nitrophenyl ester; pNPP, 4-nitrophenyl phenylphosphate.

 Published on Web 09/14/2010

Table 1: Comparison of the Enzymes in the NPP Family[a]

NPP	expression and location	substrate	reaction
NPP1	bone, and other tissues	nucleotides and derivatives	generates P_i and PP_i
NPP2 (autotoxin)	many tissues and secreted in body fluids	nucleotides and derivatives	generates P_i
		lyso-PC	cleaves choline
NPP3	intestine, basophils, mast cells, and other tissues	nucleotides and derivatives	generates P_i and PP_i
NPP4	unknown	unknown	unknown
NPP5	kidney, brain, and other tissues	unknown	unknown
NPP6	brain, kidney, and other tissues	lyso-PC, lyso-PAF	cleaves phosphocholine
		glycerophosphocholine	cleaves phosphocholine
		sphingosylphosphocholine	cleaves phosphocholine
NPP7 (alk-SMase)	intestine and human liver and secreted in gut and human bile	sphingomyelin	cleaves phosphocholine
		PAF, lyso-PC, PC	cleaves phosphocholine

[a]The table is based on the information from refs *4* and (*13*−*15*).

member that has activity against SM. To fully understand the substrate specificity, it is important to gain knowledge about the structure of the protein and the substrate binding model of the enzyme. Only recently have several high-resolution crystal structures of NPP from *Xanthomonas axonopodis* been reported (*15*), and one of them [Protein Data Bank (PDB) entry 2GSU] contains an AMP, the product of the enzyme activity. Here we present a homology model of alk-SMase based on the AMP-containing NPP crystal structure. On the basis of the model, we rationalize earlier published mutagenesis results and also propose and test additional site-directed mutageneses for altering the substrate specificity.

MATERIALS AND METHODS

The human alk-SMase sequence (Genbank accession number NP_848638, version gi 45545421) was obtained from PubMed. Cos7 cells were obtained from American Tissue Culture Collection. SM was purified from bovine milk and labeled with [^{14}C]CH_3-choline ([^{14}C]SM). The antibody against alk-SMase was raised in Agrisesa AB (Vännäs, Sweden) (*2*). The cell culture medium and other chemical agents used were purchased from Sigma. Lipofectamine and the anti-myc antibody were obtained from Invitrogen.

Homology Modeling. The human alk-SMase sequence and the template crystal structure, chain A of PDB entry 2GSU, were imported into the protein structure prediction software Prime version 2.1 (Schrödinger LLC, New York, NY). The secondary structure of alk-SMase was predicted using SSPro (*16*) and PSIPRED (*17*). The initial sequence alignment was based on both the sequence similarity and the predicted secondary structure information. Multiple iterations of manual sequence adjustments, model building, and refinement were applied until a single final model was obtained. During each iteration, the model was evaluated on the basis of a visual assessment of the quality of the alignments and protein model assessment tools such as Ramachandran Plot and Protein Report in molecular modeling interface Maestro version 9.0 (Schrödinger LLC). Before refinement, Thr75 was deprotonated on the basis of an earlier described hypothesis that it acts as a nucleophile in the reaction (*15*). Further refinement of loops and side chains was conducted using Prime. The refinement of the model was guided by the Ramachadran Plot and Protein Report tool, which showed the areas of the structure where special attention was needed. The model was processed through the Protein Preparation Wizard in Maestro to optimize the hydrogen bonding network by sampling Asn and Gln terminal rotatable bonds, predicting the best His tautomer/ionization state, and optimizing the hydrogen of the Ser/Thr hydroxyl and Cys thiol. Finally, the loop spanning Phe140 and Glu171 was predicted using the Prime loop refinement with the default protocol to generate a diverse ensemble of loop conformations. Briefly, the method builds up the loop based on a fine-grained library of backbone dihedral angles, resulting in thousands of loop conformations. The number of conformations was reduced by clustering, and representative loops were further refined by side chain prediction followed by minimization (*18*). Of the 20 different loop conformations collected, three open conformations were selected for further modeling on the basis of exposure of the pocket and glycosylation site, Asn146.

Molecular Docking. Two-dimensional (2D) or three-dimensional (3D) structures of [^{14}C]SM (PubChem CID 11433862), PAF (PubChem CID 2499), 1-palmitoylphosphatidylcholine (lyso-PC, PubChem CID 86554), and 1-palmitoyl-2-oleoylphosphatidylcholine (PC, PubChem CID 5497103) were downloaded from PubChem (http://pubchem.ncbi.nlm.nih.org). The conversion of 2D to 3D coordinates was performed using LigPrep version 2.3 (Schrödinger LLC), which also generated stereoisomers if not specified in the downloaded structures. The ionization states at the alk-SMase optimal pH of 9.0 (*2*) were assigned by Epik version 2.0 (Schrödinger LLC).

The final binding conformation of alk-SMase was generated via application of the Induced Fit Docking protocol (*19*, *20*) using SM as the ligand. Induced Fit Docking has been validated on 21 different test cases (*20*) and has been shown to generate viable binding modes in homology models (*21*−*23*). Briefly, the protocol involves three steps. First, the van der Waals radii of the active site of the enzyme and the substrate are scaled by 50%, followed by docking of the substrate saving 20 poses to thoroughly sample possible binding modes. Then, the conformations of the active site side chains are predicted with full van der Waals radii followed by a minimization of the binding site residues and ligand, generating 20 different plausible active site conformations. Finally, the substrate is docked back into these 20 active site conformations. The choice of the right complex was not trivial, as most of the binding modes were very similar and only small variations in the side chain conformations separated them. However, it is clear that for the reaction to occur, the nucleophilic Thr75 Oγ atom and the phosphorus atom of the substrates should be close. On the basis of this criterion, two complexes in which the distance was less than 4.0 Å were selected. The various substrates were then docked into the two models using Glide version 5.5 (Schrödinger LLC) (*24*, *25*) with the Standard Precision (SP) protocol. Finally, the docked substrate conformations in the binding pocket were subjected to a short minimization using

MacroModel version 9.7 (Schrödinger LLC), keeping the receptor atoms fixed. The final model was chosen on the basis of combined criteria of GlideScore and the distance from Thr75 Oγ atom to the SM phosphorus atom.

In Silico Mutation. In silico protein residue mutations were performed in Maestro, and the mutated side chain conformations were predicted using Prime, while keeping the surrounding residues fixed. Each of the mutations was visually inspected. The electrostatic potential was calculated by solving the nonlinear Poisson−Boltzmann equation in APBS (*26*) using the PyMOL version 1.2 (Schrödinger LLC) interface. Prior to the calculation in APBS, the structures were prepared by the PDB2PQR web server (*27*, *28*). The default parameters implemented in PyMOL were applied as input to APBS. These parameters included a protein dielectric constant of 2.0, a water dielectric constant of 80, a solvent radius of 1.4 Å, and a vacuum sphere density of 10 grid points/Å^2, and the equation was solved at 310 K.

Molecular Dynamics Simulation. Desmond version 2.2 (D. E. Shaw Research, New York, NY) (*29*) was used for molecular dynamics simulations of the wild-type and mutant models with the OPLS_2005 force field (*30*, *31*). The models were solvated in a TIP4P water (*32*) box with a 10 Å buffer using the System Builder module in Maestro, resulting in simulation systems of 90017 and 90019 atoms respectively. The solvated systems were relaxed via a multistage protocol starting with restrained minimization using a force constant of 50.0 kcal mol^{-1} Å^{-2} applied on solute heavy atoms. Three short simulations (48 ps in total) heated the system from 10 to 300 K while maintaining the restraint on solute heavy atoms followed by a final 24 ps preproduction simulation run at 300 K using periodic boundary conditions at a constant pressure of 1 atm using the Martyna−Tobias−Klein barostat method. Finally, the simulations were run for 1 ns each at 300 K using the Nosé-Hoover thermostat method. van der Waals and short-range electrostatic interactions were cut off at 9 Å, and the long-range electrostatic interactions were computed using the particle mesh Ewald method (*33*). A RESPA integrator (*34*) was used with a time step of 2 fs, and long-range electrostatics were computed every 6 fs.

Cell Culture and Transient Expression. The Cos7 cells were cultured in Dulbecco's modified Eagle's medium with 10% heat-inactivated fetal calf serum and 2 mM glutamine to ~90% confluence. The cells were then transfected with 4 μg of constructed plasmid with the wild-type or mutated alk-SMase cDNA insert in the presence of lipofectamine 2000, followed by incubation of the cells for 48 h, as described previously (*35*). The medium was collected, and the cells were scraped and lysed as described previously (*2*). After centrifugation at 12000*g* for 10 min at 4 °C, the cell-free extract was collected and enzyme activities were determined.

Sites-Directed Mutation. Site-directed mutagenesis was performed by the megaprimer PCR method (*36*). The oligonucleotides used for mutating the predicted active core (Met74Leu, Phe141Ser, and Phe275Gly) are listed in Table 2, in which the altered codons are underlined. The sense and antisense primers are TCGGTACCGAAAGCATGAGAGGCCCGGCCGTCCTC and TAGCGGCCGCCTGCGACCTCAGACAGAAGAAT, respectively. The mutated genes were cloned into the pcDNA4/TO/myc-His B vector at KpnI and NotI sites as the wild-type gene (*16*). Met74Leu/Phe141Ser double mutations were introduced using Met74Leu mutated alk-SMase as a template and the Phe141Ser (antisense) primer as the mutagenesis primer. After incubation for 48 h, the activities of alk-SMase from both the wild-type enzyme and the mutant were determined, and the proteins were examined by Western blotting.

Table 2: Primer Sequences Used in the Generation of the Mutant cDNA

M74L (antisense)	GAAGTGGCAGGGGCTGGT-CAGGGTGACAAAGGCGGGGGTCAT
F141S (antisense)	GGTGACGTTCCCGCCCGGGTA-GGAGAAGGAGCCAGCCCTCAGG
F275G (sense)	TTCACCTTCCGGGACATCGAG-GGTGAGCTCCTGGACTACGGACCA

alk-SMase and NPP Assays. alk-SMase activity was determined by a method described previously (*35*). Briefly, 5 μL samples were mixed with 95 μL of 50 mM Tris-HCl buffer (pH 9.0) containing 0.15 M NaCl, 2 mM EDTA, 6 mM taurocholate (assay buffer), and 0.80 μM [^{14}C]SM (~8000 dpm) and incubated at 37 °C for 30 min. The reaction was terminated by addition of 0.4 mL of a chloroform/methanol mixture (2:1) followed by centrifugation at 10000 rpm for 10 s. An aliquot (100 μL) of upper phase containing the cleaved phosphocholine was analyzed for radioactivity by liquid scintillation. In samples with high activities, 10 nmol of unlabeled SM was mixed with [^{14}C]SM to saturate the enzyme as described previously (*37*).

The nucleotidase activity was determined as described previously using both thymidine 5′-monophosphate *p*-nitrophenyl ester (pNTMP) and 4-nitrophenyl phenylphosphate (pNPP) as substrates (*2*). The activity against pNTMP was assayed in 50 mM Tris buffer (pH 8.9) containing 1 mM Zn^{2+}, and that against pNPP was in 50 mM Tris buffer (pH 8.9) containing 1 mM Ca^{2+}. The substrate concentrations for pNTMP and pNPP were 3 mM. The production of *p*-nitrophenyl was kinetically analyzed at 405 nm every 15 min up to 2 h on a microplate reader (Bio-Rad). The activity was expressed as an increment of the OD per hour per milligram of sample proteins. The protein was assessed with a kit from Bio-Rad using human albumin as a standard.

Western Blot. Western blotting for NPP7 and its mutant forms expressed in Cos7 cells were performed as described previously (*35*). The cDNAs were subcloned into expression vector pcDNA4/TO/Myc-His B. After expression, 75 μg of cellular proteins in the lysate was subjected to 10% SDS−PAGE and transferred to a nitrocellulose membrane. The membrane was probed with the anti-alk-SMase antibody (1:500) and then probed with the second antibody conjugated with horseradish peroxidase (1:50000). The protein bands were identified by enhanced chemiluminescence advance reagents, and the remitted light was recorded on Kodak X-ray film. To further confirm the results, the membrane was striped and reprobed with the anti-Myc antibody (1:5000) and then reacted with the anti-mouse IgG antibody conjugated with horseradish peroxidase. The bands were identified as described above.

RESULTS AND DISCUSSION

Homology Model. Unlike the other members of the NPP family, alk-SMase hydrolyzes SM, which is structurally very different compared to the nucleotides. The mode of binding of SM to alk-SMase cannot easily be deduced by a visual analysis of the NPP crystal structures. To understand the structure−activity relationship, we built a homology model using the structure of PDB entry 2GSU as a template, which is 27% identical in sequence. Homology models have been shown to be valuable in understanding the function of proteins (*38*) and interactions with ligands (*39*) and can even be successfully used for structure-based virtual screening (*40*, *41*).

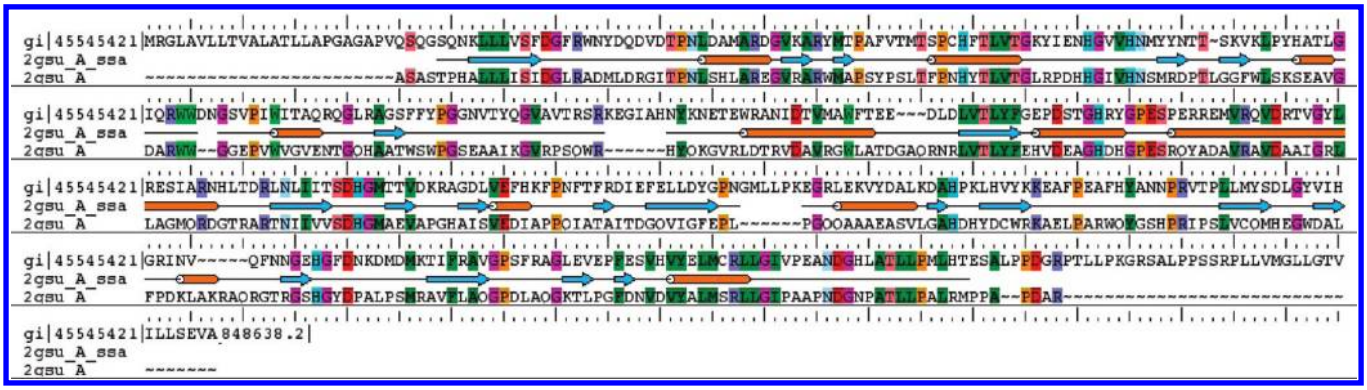

FIGURE 1: Sequence alignment of alk-SMase (gi 45545421) and *X. axonopodis* NPP 2GSU. The blue arrows indicate β-strands and orange tubes α-helices in 2GSU.

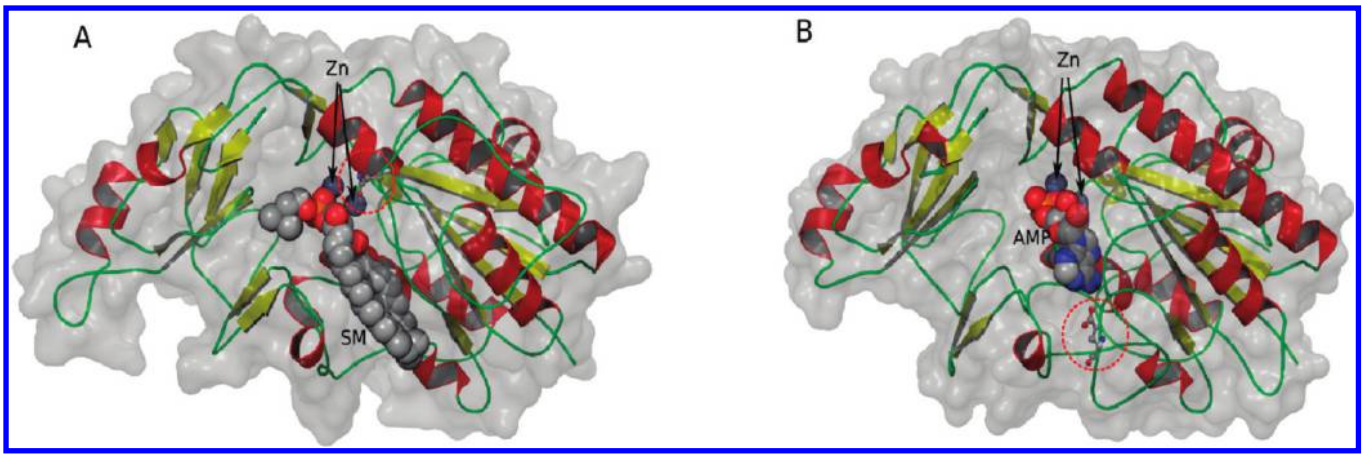

FIGURE 2: Cartoon diagram of the alk-SMase homology model (A) and the *X. axonopodis* NPP structure template 2GSU (B). The helices are colored red, β-strands yellow, and loops green. The zinc ions are shown as dark blue spheres, and ligands SM and AMP are also shown as spheres. The red circle highlights the position of glycosylated residue Asn146 (A) and its corresponding residue in 2GSU, Glu160 (B). In the NPP template (B), this position is partially buried and therefore is not accessible for glycosylation, whereas in alk-SMase (A), it is fully exposed. The ligands show the extent of the binding pocket that is more elongated in alk-SMase than NPP.

The AMP-bound *X. axonopodis* NPP crystal structure of PDB entry 2GSU contains two similar chains (*15*). In this study, we chose to base our model on chain A of 2GSU (2GSU:A) as chain B presents an unlikely close contact between Thr75 Oγ and a phosphate oxygen atom (1.8 Å). The final sequence alignment is shown in Figure 1. The initial model presented two major issues. First, the binding site of the template is too short to accommodate the long tails of SM because of blockage by a semiburied long loop containing residues 140−171. An earlier experiment also showed that in alk-SMase, a glycosylation site (Asn146) is located in the middle of the loop (*35*) and therefore must be fully exposed to the solvent. Interestingly, the corresponding loop is much shorter in NPP2, which also binds phospholipids, and the short loop would expose a narrow channel of the binding pocket. The evidence suggests that this loop in alk-SMase will assume an open conformation as opposed to the template. Using the hierarchical loop sampling method in Prime, we collected different loop conformations and selected only low-energy conformations that have an open narrow hydrophobic channel in the binding site and at the same time expose Asn146 to the solvent. Accurately modeling such a long loop is a computational challenge, but our goal is to generate the most diverse loop conformations possible. Although long loops can be sampled with other simulation methods such as molecular dynamics and Monte Carlo simulations, the Prime hierarchical loop sampling method can produce diverse loop conformations within a few hours on a single CPU (*18*). Second, the active site in the initial model does not readily accommodate SM; therefore, a plausible bioactive conformation of the binding site needed to be calculated via application of the Induced Fit Docking protocol (*19*) using SM as an inducing agent.

On the basis of the approach described above, the final model of alk-SMase is shown in Figure 2 along with the template bacterial crystal structure. The active site is situated between two domains. The smaller domain has a five-strand plated sheet with two very short helices packed loosely to it, and the larger domain is an α−β−α sandwich structure. The superposition on the template crystal structure shows a dramatic conformational change of the loop of residues 140−171 in alk-SMase where Asn146 was exposed on the surface (Figure 2A), whereas the corresponding residue in the bacterial NPP, Glu160, is partially buried (Figure 2B). Two active site zinc ions are coordinated by Asp199, His203, His353, His247, Asp39, Asp246, and Thr75. It was hypothesized that the Zn ions probably extract a proton from the catalytic threonine in NPPs, producing a negatively charged alkoxide (*15*). The hypothesis was based on the pH profile analysis of catalytic activity of a similar catalytic serine in homologous alkaline phosphatase (*42*). By analogy, the pK_a of Thr75 in alk-SMase is expected to be in the same range, and at the alk-SMase optimal pH of 9, it is expected to be negatively charged and was modeled as such.

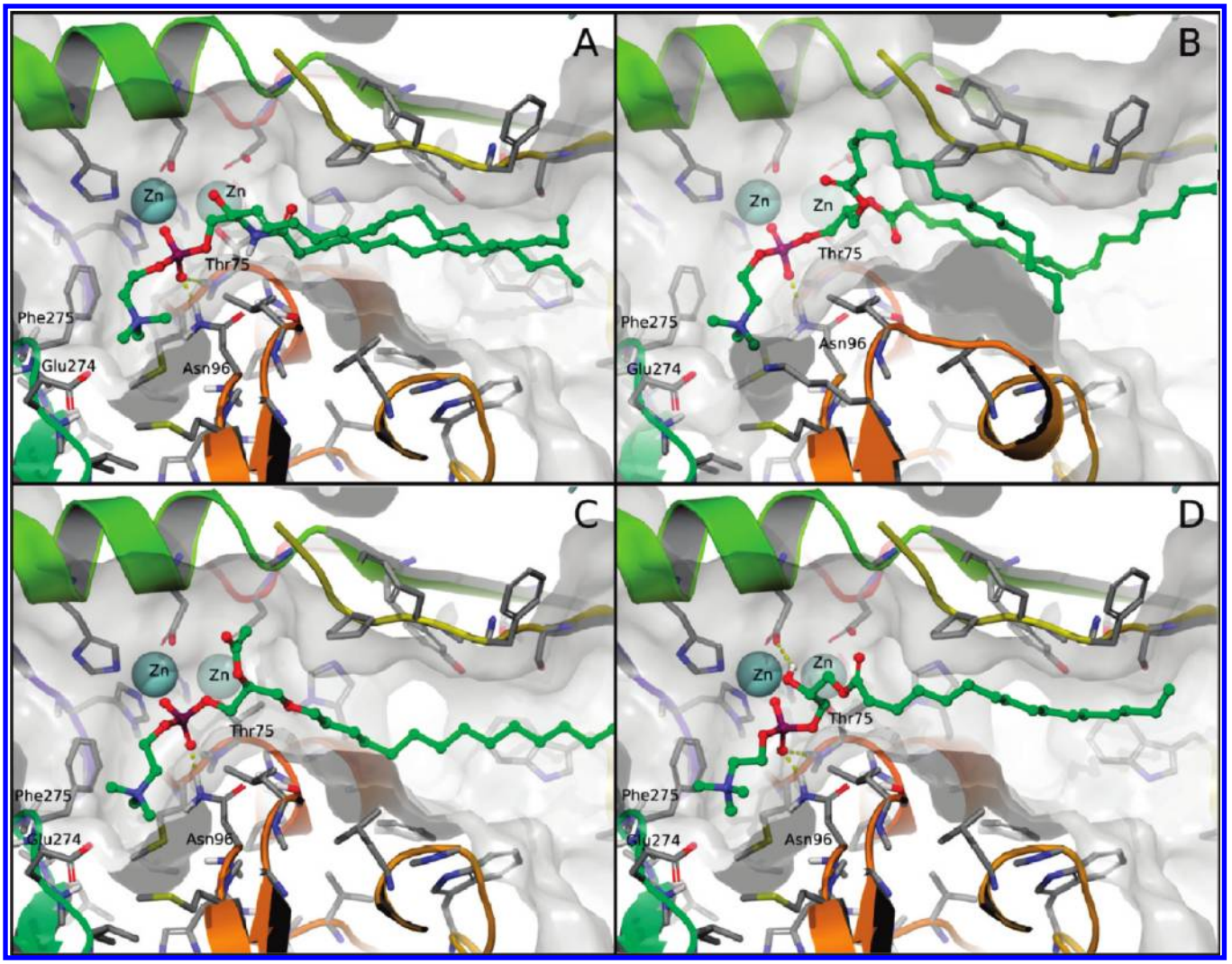

FIGURE 3: Substrate binding mode as predicted by docking for (A) SM, (B) PC, (C) PAF, and (D) lyso-PC. The binding mode is essentially conserved across all four substrates where one of the oxygen atoms of the phosphate groups is coordinated to the Zn ions while the other one forms hydrogen bonds (yellow dashed lines) to Asn96 and the backbone of Thr75. The binding of the choline groups is stabilized by a salt bridge to Asp274 and van der Waals interaction with Phe275. The aliphatic tails of these molecules are extended in a narrow groove of the enzyme.

Predicted Substrate Binding Mode. SM was docked into the long narrow channel consisting of a polar activity pocket around the Zn ions and a narrow hydrophobic groove. The phosphocholine group of SM is located in the activity pocket where the choline headgroup interacts with Phe275 and forms a salt bridge with Glu274 (Figure 3A). The phosphate group is coordinated to a Zn ion, and the distance between Thr75 Oγ and SM phosphorus is ~3.7 Å, similar to the distance found in the template *X. axonopodis* NPP structure (3.2 Å) (*15*). The phosphate also forms two hydrogen bonds to the Thr75 backbone amine and Asn96 side chain (Figure 3A). The hydrogen bonding interaction with Asn96 is important for the hydrolysis as it provides stabilization for the transition state (*15*). The long alkyl tails of SM lie in the hydrophobic groove (Figure 3A), and interactions there are dominated by nonspecific hydrophobic and van der Waals contacts. PC, PAF, and lyso-PC exhibit essentially the same binding mode as SM (Figure 3B−D).

We previously showed that alk-SMase, although related to NPPs, has no activity against nucleotides (*2*). Our model may provide an explanation for such a property. The main interactions in the phosphate binding site are essentially the same. These include coordination to the ions, interaction with Thr75, and a hydrogen bond to Asn96. However, several stabilizing interactions for the base are missing in the alk-SMase structure because of a change in loop conformation. In template 2GSU, the nucleotide base is stabilized by a hydrogen bond to Glu160, a coplanal $\pi-\pi$ stacking interaction with Tyr174, and an edge-to-face interaction with Phe91. The two first residues were functionally conserved (Glu160 was exchanged with an asparagine in alk-SMase, and Tyr174 was not exchanged at all); however; both were located in the long loop. Phe91 was mutated to serine, which does not allow the same favorable aromatic interaction. In the next section, we closely examine the effect of such a mutation.

Model Explaining the Structure−Activity Relationship. Our early study of site mutations in the active core such as Met74Lys, Thr75Ala, Ser76Phe, and Cys78Asn showed loss of alk-SMase activity against SM and still no increase in activity against nucleotides (*35*). Here we introduced the same in silico mutations, and the new side chain conformations were predicted and are shown in Figure 4. Met74Lys introduced a positive charge, and the Lys side chain was predicted to be plugged into a hydrophobic pocket surrounded by Val72, Ile273, Phe275, and Leu277, although one hydrogen bond was predicted between the Lys and a backbone carbonyl (Figure 4A). Without balancing charges or additional hydrogen bonds, the desolvation penalty for burying a lysine will be much larger than the favorable

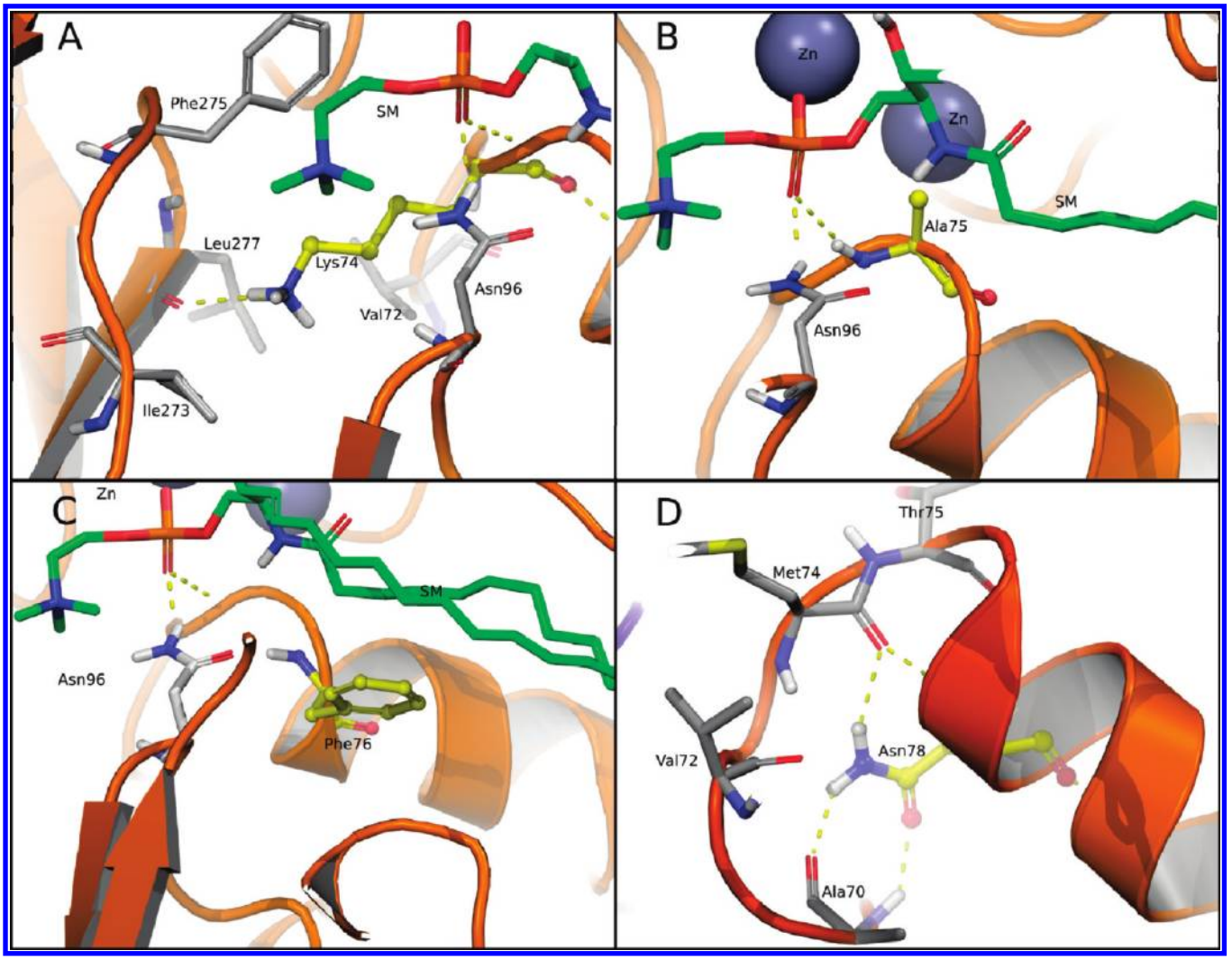

FIGURE 4: (A) Met74Lys mutation that causes electrostatic repulsion with the ligand choline group and also introduction of charges into the overall hydrophobic environment. (B) Thr75Ala mutation that has a direct impact on the catalysis as the oxygen atom responsible for nucleophilic attack is removed. (C) Ser76Phe mutation that causes steric clash with the tails of the substrate but also a stabilizing hydrogen bond from the wild-type serine residue to Asn96 removed by the mutation. (D) Cys78Asn mutation that introduces three hydrogen bonds into backbone groups of Met74 and Ala70. In this figure, the hydrogen bonds are shown as dashed yellow lines. The mutated residues are shown as yellow balls and sticks.

interaction. Further, the proximity to the choline group of the ligand can cause strong electrostatic repulsion, thus explaining why there is no activity toward SM. Analogous to alkaline phosphatase, it was proposed that Thr75 is directly involved in the reaction via the attack of a nucleophile on the ligand phosphorus atom (*15*). Thr75Ala would remove all activity by simply removing the nucleophilic group directly responsible for the reaction (Figure 4B). The result further supports the hypothesis that alk-SMase shares the same mechanism as alkaline phosphatase. The Ser76Phe (Figure 4C) substitution was designed to restore the edge-to-face interaction to the nucleotide described earlier. The corresponding residue in the template is Phe91. The substitution placed a large bulky residue into the hydrophobic channel clashing with the SM alkyl chain and at the same time removing a stabilizing hydrogen bond between Ser76 and the Asn96 side chain. Therefore, this mutation has both adverse binding and catalytic effects on SM hydrolysis. As expected, no SM hydrolysis activity was observed, and unfortunately, no activity toward nucleotides was observed. As for the Cys78Asn mutation (Figure 4D), the effect seems to be more subtle. Introduction of Asn resulted in hydrogen bonds with the Ala70 backbone carbonyl and amine and Met74 carbonyl that should stabilize the important loop where the catalytic Thr75 is located (Figure 4B). However, stabilization also means that the loop is more rigid, and considering SM is much more flexible than nucleotides, the rigidity of the loop may have an impact on SMase activity.

Comparison of the Predicted Structure of alk-SMase and NPP at Positions 74, 275, and 141. The previously published mutations were designed on the basis of sequence alignment without a structural model. A close comparison between the alk-SMase model and the 2GSU template revealed a couple of interesting sites. Met74 in alk-SMase seemed to introduce some strain into surrounding residues, in particular, Asn96, which stabilizes the transition state by forming hydrogen bonds to the phosphate (*15*). A substitution of Met74 with the corresponding side chain in 2GSU, Leu, might relieve the strain and allows Asn96 to adopt a more stable conformation for forming hydrogen bonds to the substrate (Figure 5A). According to the docked pose, Phe275 in alk-SMase is in van der Waals contact with methyl groups in the phosphocholine group of the substrate (Figures 3A and 4A), and it would not provide good interaction with di- or triphosphates in nucleotides. In 2GSU, it is substituted with Gly, thus creating space for the phosphates to fit.

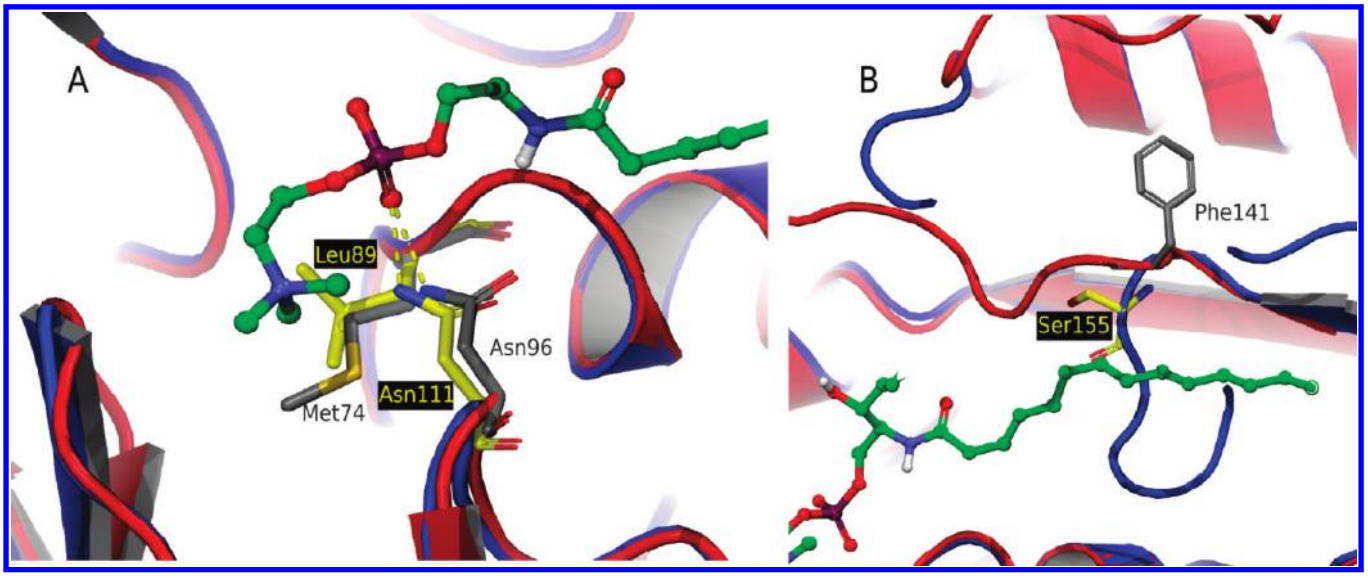

FIGURE 5: alk-SMase cartoon (red) and atoms (gray) and NPP cartoon (blue) and atoms (yellow). The text colors follow the atom color. (A) Comparison of alk-SMase and NPP template structure at position 74 of alk-SMase. The larger side chain of Met74 pushes Asn96 away from the optimal hydrogen bonding position compared to NPP. (B) The same comparison at position 141 of alk-SMase, where Ser155 in NPP induced a turn in the loop while the loop in alk-SMase was predicted to be extended at the corresponding position.

Finally, a crucial difference between our model and the template is the loop of residues 140−171. In our model, the loop was predicted to extend along the side of the hydrophobic ligand binding channel, but in the *X. axonopodis* NPP template, a 90° bend turned the loop back into the channel. The bend was located on a serine in the NPP template that was substituted with Phe141 in our model, and the large side chain of the phenylalanine probably prevented the loop from turning (Figure 5B). If we substitute Phe141 with serine, the loop might again adopt the same conformation as in the template NPP structure.

Identification of an Activity-Increasing Mutation. On the basis of the comparison and discussion, we can predict that the effect of the three mutations would likely be the loss of activity for SM and an increase in activity for nucleotides. We therefore introduced Met74Leu, Phe275Gly, and Phe141Ser mutations. The two last mutant enzymes were found to have no activity against SM as expected. Surprisingly, the Met74Leu mutant had ~75% higher SMase activity than the wild type at alkaline pH when measured in the presence of 100 pM [^{14}C]SM (Figure 6). However, when the activity was assayed in the presence of 10 nM SM, the activity of Met74Leu was found to be increased by 188%. The result prompted us to investigate this mutant further using molecular dynamics simulations, which can be used to explain protein structure−function problems, such as folding, stability, and mutational effects (*43*−*46*). In the simulations, we monitored the hydrogen bonding distance between Asn96 and the phosphate group for both the wild type and the mutant, and as expected, this hydrogen bond is less conserved in wild-type alk-SMase than in the Met74Leu mutant (Figure 7). The result supports our hypothesis that the Met74Leu mutation influences the activity indirectly through Asn96. Unfortunately, all three also showed no activity for nucleotides. To investigate synergy effects, we also created double mutant Met74Leu/Phe141Ser and the triple mutant, none of which had activity against nucleotide or SM (Table 3). It seems that either re-creation of the template loop conformation was not successful or there are other factors not addressed by the mutations.

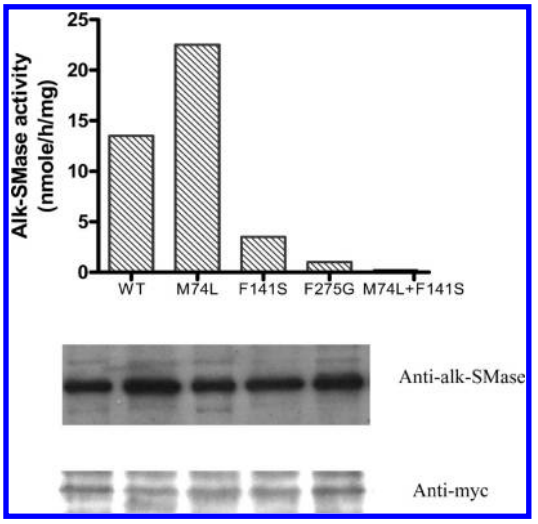

FIGURE 6: alk-SMase activity measurement for mutants Met74Leu, Phe141Ser, Phe275Gly, and Met74Leu/Phe141Ser. The constructed cDNAs of both the wild type and the mutants were cloned into vector pcDNA4/TO/myc-His B and induced into Cos7 cells. The cell lysates 48 h after the transfection were prepared, and the alk-SMase activities were determined using 100 pmol of choline-labeled [^{14}C]SM as the substrate. The activities were adjusted with the protein levels in the lysate. The bottom panels show the results of the Western blot against both alk-SMase and Myc protein to check the efficiency of the transfection as the vector is myc-linked.

The site-directed mutagenesis results show that substrate specificity cannot be easily changed by a few mutations around the binding site and the active center. Residues farther from the binding pocket can also contribute significantly. By displaying the electrostatic potential on the molecular surface, we noticed a much stronger positive potential in *X. axonopodis* NPP roughly 16−18 Å from the phosphate groups (Figure 8A). This area covers a loop of residues 348−360 in NPP and contains multiple positively charged residues: Lys350, Lys353, Arg354, Arg357, and Arg360. This unusual cluster is absent in alk-SMase (Figure 8B) and may provide stabilization for the di- and triphosphate groups via long-range charge−charge interactions.

Table 3: Activities (ΔOD_{405} per hour per milligram) of Mutant Forms of alk-SMase against pNPP and pNTMP[a]

	against pNPP	against pNTMP	*n*
control	0.881 ± 0.011	1.351 ± 0.065	4
wild type	0.760 ± 0.017	1.054 ± 0.057	3
M74L	0.814 ± 0.031	1.208 ± 0.032	4
F275G	0.704 ± 0.035	0.952 ± 0.060	3
F141S	0.946 ± 0.054	1.208 ± 0.030	4
M74L/F141S	0.663 ± 0.017	0.762 ± 0.048	3

[a]Cos7 cells were transfected with the empty vector (control) or vectors inserted with the cDNA of the wild type (WT) and various mutant forms of alk-SMase for 48 h. The NPP activities of the cell extract against pNPP and pNTMP were determined. The activities were expressed as the increment of the optical densities at 405 mm in 1 h and were adjusted to the protein levels in the samples. Results are means ± the standard error of the mean obtained from three to four separate transfections (*n*). No statistical significance was identified in any of the mutant forms compared with the control.

Similar "action-at-a-distance" interactions have been reported previously (*47*), which provides a basis for this hypothesis. Additionally, this loop is also shortened in alk-SMase. In a full attempt to re-engineer nucleotide activity in alk-SMase, one should not only mutate residues in the catalytic core as described previously but also re-create the positive charge cluster. However, this task is beyond the scope of this study.

In conclusion, this paper provides a predicted structural model of alk-SMase ligand interaction, the only NPP member with activity against SM but not nucleotide, through molecular modeling. The model largely explains the substrate specificity and the previous mutagenesis results. It may aid in understanding the substrate specificity of various members of the NPP family. The study also identified a mutation that can increase the alk-SMase activity by almost 3-fold, which may have clinical implications, as recombinant alk-SMase has been shown to suppress inflammatory bowel diseases (*10*, *12*).

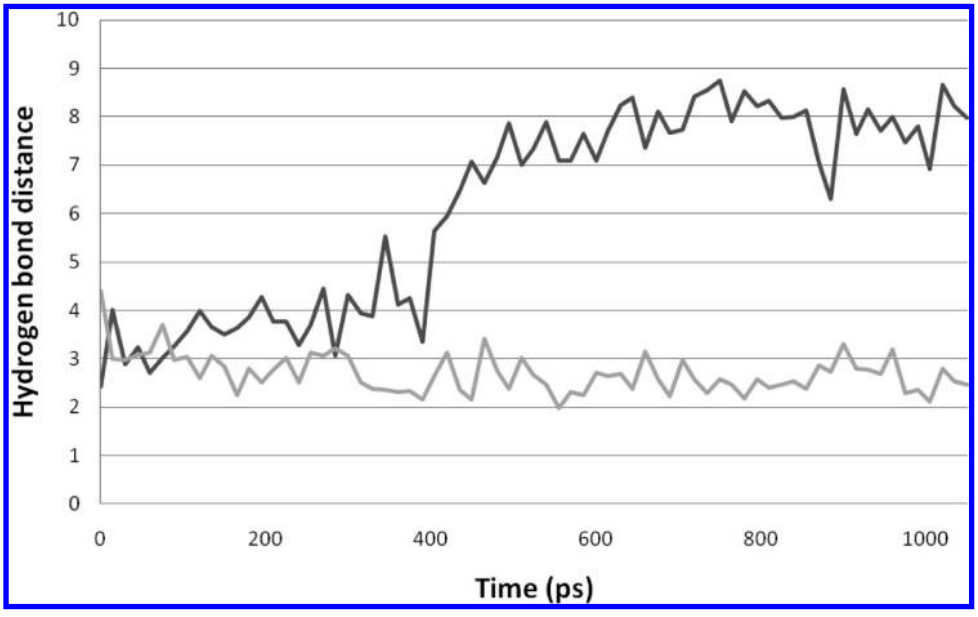

FIGURE 7: Hydrogen bonding distance between the Asn96 side chain amine hydrogen atom and the phosphate oxygen atom monitored during the molecular dynamics simulations. The black line is from the wild-type simulation, and the gray line is from the Met74Leu mutant simulation. At ~400 ps, the Asn96 side chain turned away from phosphate group in the wild-type simulation while the hydrogen bond was maintained in the Met74Leu mutant simulation.

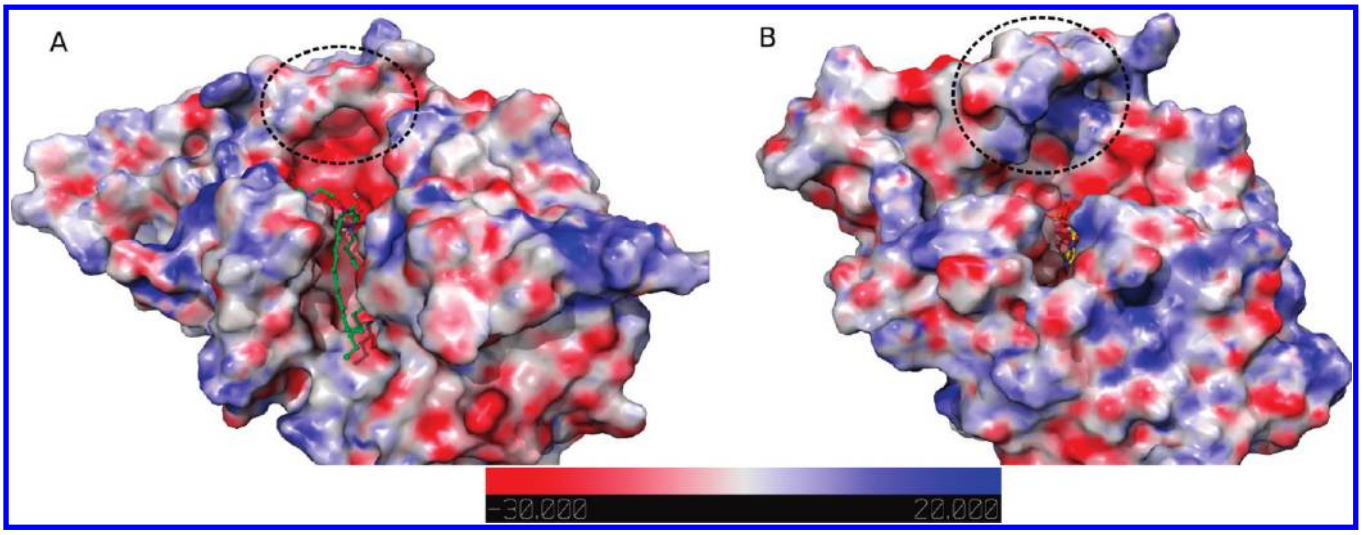

FIGURE 8: Protein electrostatic potential calculated with APBS mapped onto the molecular surface of the alk-SMase model (A) and the *X. axonopodis* NPP crystal structure (B). Blue indicates positive potentials up to $20kT$ and red negative potentials up to $-30kT$. The ligands SM and AMP are shown as sticks. Close to the ligand phosphocholine and phosphate headgroups, the electrostatic potentials are very different (highlighted in circles). The NPP structure has positive potential, while alk-SMase demonstrates negative potential.

ACKNOWLEDGMENT

We thank Dr. Åke Nilsson for valuable discussions and suggestions and Dr. Woody Sherman for helpful comments in the preparation of the manuscript.

REFERENCES

1. Nilsson, Å. (1969) The presence of sphingomyelin- and ceramide-cleaving enzymes in the small intestinal tract. *Biochim. Biophys. Acta 176*, 339–347.
2. Duan, R. D., Bergman, T., Xu, N., Wu, J., Cheng, Y., Duan, J., Nelander, S., Palmberg, C., and Nilsson, A. (2003) Identification of Human Intestinal Alkaline Sphingomyelinase as a Novel Ecto-enzyme Related to the Nucleotide Phosphodiesterase Family. *J. Biol. Chem. 278*, 38528–38536.
3. Wu, J., Nilsson, A., Jonsson, B. A., Stenstad, H., Agace, W., Cheng, Y., and Duan, R. D. (2006) Intestinal alkaline sphingomyelinase hydrolyses and inactivates platelet-activating factor by a phospholipase C activity. *Biochem. J. 394*, 299–308.
4. Duan, R. D. (2006) Alkaline sphingomyelinase: An old enzyme with novel implications. *Biochim. Biophys. Acta 1761*, 281–291.
5. Hertervig, E., Nilsson, A., Bjork, J., Hultkrantz, R., and Duan, R. D. (1999) Familial adenomatous polyposis is associated with a marked decrease in alkaline sphingomyelinase activity: A key factor to the unrestrained cell proliferation? *Br. J. Cancer 81*, 232–236.
6. Hertervig, E., Nilsson, A., Nyberg, L., and Duan, R. D. (1997) Alkaline sphingomyelinase activity is decreased in human colorectal carcinoma. *Cancer 79*, 448–453.
7. Sjöqvist, U., Hertervig, E., Nilsson, A., Duan, R. D., Ost, A., Tribukait, B., and Lofberg, R. (2002) Chronic colitis is associated with a reduction of mucosal alkaline sphingomyelinase activity. *Inflammatory Bowel Dis. 8*, 258–263.
8. Cheng, Y., Wu, J., Hertervig, E., Lindgren, S., Duan, D., Nilsson, A., and Duan, R. D. (2007) Identification of aberrant forms of alkaline sphingomyelinase (NPP7) associated with human liver tumorigenesis. *Br. J. Cancer 97*, 1441–1448.
9. Wu, J., Cheng, Y., Nilsson, A., and Duan, R. D. (2004) Identification of one exon deletion of intestinal alkaline sphingomyelinase in colon cancer HT-29 cells and a differentiation-related expression of the wild-type enzyme in Caco-2 cells. *Carcinogenesis 25*, 1327–1333.
10. Andersson, D., Kotarsky, K., Wu, J., Agace, W., and Duan, R. D. (2009) Expression of alkaline sphingomyelinase in yeast cells and anti-inflammatory effects of the expressed enzyme in a rat colitis model. *Dig. Dis. Sci. 54*, 1440–1448.
11. Zhang, P., Li, B., Gao, S., and Duan, R. D. (2008) Dietary sphingomyelin inhibits colonic tumorigenesis with an up-regulation of alkaline sphingomyelinase expression in ICR mice. *Anticancer Res. 28*, 3631–3635.
12. Soo, I., Madsen, K. L., Tejpar, Q., Sydora, B. C., Sherbaniuk, R., Cinque, B., Di Marzio, L., Cifone, M. G., Desimone, C., and Fedorak, R. N. (2008) VSL#3 probiotic upregulates intestinal mucosal alkaline sphingomyelinase and reduces inflammation. *Can. J. Gastroenterol. 22*, 237–242.
13. Stefan, C., Jansen, S., and Bollen, M. (2005) NPP-type ectophosphodiesterases: Unity in diversity. *Trends Biochem. Sci. 30*, 542–550.
14. Sakagami, H., Aoki, J., Natori, Y., Nishikawa, K., Kakehi, Y., and Arai, H. (2005) Biochemical and molecular characterization of a novel choline-specific glycerophosphodiester phosphodiesterase belonging to the nucleotide pyrophosphatase/phosphodiesterase family. *J. Biol. Chem. 280*, 23084–23093.
15. Zalatan, J. G., Fenn, T. D., Brunger, A. T., and Herschlag, D. (2006) Structural and functional comparisons of nucleotide pyrophosphatase/phosphodiesterase and alkaline phosphatase: Implications for mechanism and evolution. *Biochemistry 45*, 9788–9803.
16. Pollastri, G., Przybylski, D., Rost, B., and Baldi, P. (2002) Improving the prediction of protein secondary structure in three and eight classes using recurrent neural networks and profiles. *Proteins 47*, 228–235.
17. Jones, D. T. (1999) Protein secondary structure prediction based on position-specific scoring matrices. *J. Mol. Biol. 292*, 195–202.
18. Jacobson, M. P., Pincus, D. L., Rapp, C. S., Day, T. J., Honig, B., Shaw, D. E., and Friesner, R. A. (2004) A hierarchical approach to all-atom protein loop prediction. *Proteins 55*, 351–367.
19. Sherman, W., Beard, H. S., and Farid, R. (2006) Use of an induced fit receptor structure in virtual screening. *Chem. Biol. Drug Des. 67*, 83–84.
20. Sherman, W., Day, T., Jacobson, M. P., Friesner, R. A., and Farid, R. (2006) Novel procedure for modeling ligand/receptor induced fit effects. *J. Med. Chem. 49*, 534–553.
21. Celik, L., Sinning, S., Severinsen, K., Hansen, C. G., Moller, M. S., Bols, M., Wiborg, O., and Schiott, B. (2008) Binding of serotonin to the human serotonin transporter. Molecular modeling and experimental validation. *J. Am. Chem. Soc. 130*, 3853–3865.
22. Koldso, H., Severinsen, K., Tran, T. T., Celik, L., Jensen, H. H., Wiborg, O., Schiott, B., and Sinning, S. (2010) The two enantiomers of citalopram bind to the human serotonin transporter in reversed orientations. *J. Am. Chem. Soc. 132*, 1311–1322.
23. Xing, L., Kurumbail, R. G., Frazier, R. B., Davies, M. S., Fujiwara, H., Weinberg, R. A., Gierse, J. K., Caspers, N., Carter, J. S., McDonald, J. J., Moore, W. M., and Vazquez, M. L. (2009) Homotimeric structural model of human microsomal prostaglandin E synthase-1 and characterization of its substrate/inhibitor binding interactions. *J. Comput.-Aided Mol. Des. 23*, 13–24.
24. Friesner, R. A., Banks, J. L., Murphy, R. B., Halgren, T. A., Klicic, J. J., Mainz, D. T., Repasky, M. P., Knoll, E. H., Shelley, M., Perry, J. K., Shaw, D. E., Francis, P., and Shenkin, P. S. (2004) Glide: A new approach for rapid, accurate docking and scoring. 1. Method and assessment of docking accuracy. *J. Med. Chem. 47*, 1739–1749.
25. Halgren, T. A., Murphy, R. B., Friesner, R. A., Beard, H. S., Frye, L. L., Pollard, W. T., and Banks, J. L. (2004) Glide: A new approach for rapid, accurate docking and scoring. 2. Enrichment factors in database screening. *J. Med. Chem. 47*, 1750–1759.
26. Baker, N. A., Sept, D., Joseph, S., Holst, M. J., and McCammon, J. A. (2001) Electrostatics of nanosystems: Application to microtubules and the ribosome. *Proc. Natl. Acad. Sci. U.S.A. 98*, 10037–10041.
27. Dolinsky, T. J., Czodrowski, P., Li, H., Nielsen, J. E., Jensen, J. H., Klebe, G., and Baker, N. A. (2007) PDB2PQR: Expanding and upgrading automated preparation of biomolecular structures for molecular simulations. *Nucleic Acids Res. 35*, W522–W525.
28. Dolinsky, T. J., Nielsen, J. E., McCammon, J. A., and Baker, N. A. (2004) PDB2PQR: An automated pipeline for the setup of Poisson-Boltzmann electrostatics calculations. *Nucleic Acids Res. 32*, W665–W667.
29. Bowers, K. J., Chow, E., Xu, H., Dror, R. O., Eastwood, M. P., Gregersen, B. A., Klepeis, J. L., Kolossary, I., Moraes, M. A., Sacerdoti, F. D., Salmon, J. K., Shan, Y., and Shaw, D. E. (2006) Scalable algorithms for molecular dynamics simulations on commodity clusters. In Proceedings of the 2006 ACM/IEEE Conference on Supercomputing (SC06), Association for Computing Machinery.
30. Jorgensen, W. L., Maxwell, D. S., and Tirado-Rives, J. (1996) Development and testing of the OPLS all-tom force field on conformational energetics and properties of organic liquids. *J. Am. Chem. Soc. 118*, 11225–11236.
31. Kaminski, G., Friesner, R. A., Tirado-Rives, J., and Jorgensen, W. L. (2001) Evaluation and reparameterization of the OPLS-AA force field for proteins via comparison with accurate quantum chemical calculations on peptides. *J. Phys. Chem. B 105*, 6474–6487.
32. Jorgensen, W. L., and Madura, J. D. (1985) Temperature and size dependence for Monte Carlo simulations of TIP4P water. *Mol. Phys. 56*, 1381.
33. Darden, T., York, D., and Pedersen, L. (1993) Particle mesh Ewald: An N-log(N) method for Ewald sums in large systems. *J. Chem. Phys. 98*, 10089–10092.
34. Tuckerman, M., Berne, B. J., and Martyna, G. J. (1992) Reversible multiple time scale molecular dynamics. *J. Chem. Phys. 97*, 1990–2001.
35. Wu, J., Hansen, G. H., Nilsson, A., and Duan, R. D. (2005) Functional studies of human intestinal alkaline sphingomyelinase by deglycosylation and mutagenesis. *Biochem. J. 386*, 153–160.
36. Giebel, L. B., and Spritz, R. A. (1990) Site-directed mutagenesis using a double-stranded DNA fragment as a PCR primer. *Nucleic Acids Res. 18*, 4947.
37. Duan, R. D., and Nilsson, A. (2000) Sphingolipid hydrolyzing enzymes in the gastrointestinal tract. *Methods Enzymol. 311*, 276–286.
38. Duan, J., Dahlback, B., and Villoutreix, B. O. (2001) Proposed lipocalin fold for apolipoprotein M based on bioinformatics and site-directed mutagenesis. *FEBS Lett. 499*, 127–132.
39. Nilsson, A., Duan, J., Mo-Boquist, L. L., Benedikz, E., and Sundstrom, E. (2007) Characterisation of the human NMDA receptor subunit NR3A glycine binding site. *Neuropharmacology 52*, 1151–1159.
40. Bissantz, C., Schalon, C., Guba, W., and Stahl, M. (2005) Focused library design in GPCR projects on the example of 5-HT(2c) agonists: Comparison of structure-based virtual screening with ligand-based search methods. *Proteins 61*, 938–952.
41. Evers, A., and Klabunde, T. (2005) Structure-based drug discovery using GPCR homology modeling: Successful virtual screening for antagonists of the α1A adrenergic receptor. *J. Med. Chem. 48*, 1088–1097.

42. O'Brien, P. J., and Herschlag, D. (2002) Alkaline phosphatase revisited: Hydrolysis of alkyl phosphates. *Biochemistry 41*, 3207–3225.
43. Duan, J., and Nilsson, L. (2002) The role of residue 50 and hydration water molecules in homeodomain DNA recognition. *Eur. Biophys. J. 31*, 306–316.
44. Duan, J., and Nilsson, L. (2005) Thermal unfolding simulations of a multimeric protein: Transition state and unfolding pathways. *Proteins 59*, 170–182.
45. Duan, J., and Nilsson, L. (2006) Effect of Zn^{2+} on DNA recognition and stability of the p53 DNA-binding domain. *Biochemistry 45*, 7483–7492.
46. Lee, E. H., Hsin, J., Sotomayor, M., Comellas, G., and Schulten, K. (2009) Discovery through the computational microscope. *Structure 17*, 1295–1306.
47. Joughin, B. A., Green, D. F., and Tidor, B. (2005) Action-at-a-distance interactions enhance protein binding affinity. *Protein Sci. 14*, 1363–1369.